

On-the-fly machine learning for parametrization of the effective Hamiltonian

Xingyue Ma,^{1,2} L. Bellaiche,³ Di Wu,^{1,2,*} and Yurong Yang^{1,2,†}

¹*National Laboratory of Solid State Microstructures and Collaborative Innovation Center of Advanced Microstructures, Nanjing University, Nanjing 210093, China*

²*Jiangsu Key Laboratory of Artificial Functional Materials,*

Department of Materials Science and Engineering, Nanjing University, Nanjing 210093, China

³*Physics Department and Institute for Nanoscience and Engineering, University of Arkansas, Fayetteville, Arkansas 72701, USA*

(Dated: July 19, 2023)

The first-principles-based effective Hamiltonian is widely used to predict and simulate the properties of ferroelectrics and relaxor ferroelectrics. However, the parametrization method of the effective Hamiltonian is complicated and hardly can resolve the systems with complex interactions and/or complex components. Here, we developed an on-the-fly machine learning approach to parametrize the effective Hamiltonian based on Bayesian linear regression. The parametrization is completed in molecular dynamics simulations, with the energy, forces and stress predicted at each step along with their uncertainties. First-principles calculations are executed when the uncertainties are large to retrain the parameters. This approach provides a universal and automatic way to compute the effective Hamiltonian parameters for any considered systems including complex systems which previous methods can not handle. BaTiO₃ and Pb(Sc, Ta)O₃ are taken as examples to show the accurateness of this approach comparing with conventional first-principles parametrization method.

I. INTRODUCTION

First-principles (FP) calculations based on density functional theory (DFT) [1, 2] is a powerful tool for computing structures and properties of various materials [3]. However, computing the finite temperature properties, such as the phase transitions induced by temperature, remains a great challenge due to the large computational cost required. To compute the finite temperature properties within affordable computational costs, several first-principles-based state-of-art computational approaches have been developed. One important example is the first-principles-based effective Hamiltonian approach designed for ferroelectric related materials (mostly perovskite compounds with the form ABX₃) [4, 5], which has been developed and used for a large number of materials, such as BaTiO₃ [4], Pb(Zr, Ti)O₃ [6, 7], KNbO₃ [8], CsPbI₃ [9] and so on. Monte Carlo (MC) and molecular dynamics (MD) simulations based on the effective Hamiltonian have successfully reproduced or predicted phase transitions [10], topological defects [11, 12], dielectric response [13], piezoelectric effect [14], electrocaloric effect [15, 16], optical response [8], and the effect of atomic ordering [17, 18].

The effective Hamiltonian is built up based on the Taylor expansion of small atomic distortions on energy around a selected high symmetry reference structure, and the expansion parameters are typically fitted by performing FP calculations on several small cells with specially designed atomic distortions [4, 19]. However, the fitting and verifying of the parameters are not easy tasks, especially for systems with complex interactions. Additional manual adjusting the values of some specified parameters may be necessary to reproduce some experimental results correctly [8, 20], which may be re-

sulted from the large uncertainty arisen from the parametrization process [8]. Moreover, for complex perovskites with multi elements in *A* or *B* sites [such as (Ba, Sr)TiO₃ and Pb(Zr, Ti)O₃], the effective Hamiltonian is usually built up by applying virtual crystal approximation (VCA) and a small amount of simple terms that dependent explicitly on the atomic distributions [6, 21, 22]. Such approximations and the difficulty of parametrization in complex systems limit the effective Hamiltonian for perovskites with relatively simple components (mostly up to only two different elements in *A* or *B* site).

Recently, high entropy materials have attracted great attention due to their excellent mechanical and physical properties [23–26]. Some “high entropy perovskites” or perovskites with complex components are also found to have excellent performance of energy storage [27, 28] and electrocaloric effect [29]. Modeling these high entropy materials with first-principles-based models such as the effective Hamiltonian is of great interest to understand their properties and design new functional materials. However, modeling such complex systems is a great challenge with currently available effective Hamiltonian model and parametrization methods. Thus, finding a new scheme for fitting the parameters of effective Hamiltonian in a reliable and automatic way is highly demanded.

The development of first-principles-based machine learning force fields (MLFFs) in recent years demonstrates the efficiency and reliability of on-the-fly active learning methods for training the force fields [30–35]. In these methods, the data selection and training are completed during an MD simulation based on the force field. The energy, forces and stress as well as their uncertainties are predicted by the force field. If the predicted uncertainty is small, the MD simulation continues with the forces and stress predicted by the force field. Otherwise, FP calculation is performed to retrain the force field, and the MD simulation continues with the forces and stress obtained from the FP calculation [30–32].

In this article, on-the-fly active learning method is applied

* diwu@nju.edu.cn

† yangyr@nju.edu.cn

to the parametrization of the effective Hamiltonian for perovskite structures. In Sec. II, the formalism of the effective Hamiltonian and the on-the-fly machine learning algorithm are present in detail. In Sec. III, the computational details of the example are described. In Sec. IV, the example of Pb(Sc, Ta)O₃ is presented. Finally, Sec. V summarizes this work.

II. FORMALISM

In this section, the outline of the on-the-fly machine learning scheme is first presented. Then the expression of the effective Hamiltonian employed here are reviewed with several new terms. After showing the formalism of linkage between the effective Hamiltonian and FP calculations, the formalism of the parametrization and the strategy of the decisions to do FP calculations are shown, with stressed special features of the effective Hamiltonian and the differences from the MLFF schemes. Finally, special discussions are given on the multi component perovskites.

A. Outline of the on-the-fly fitting scheme

In our approach, the parameters of effective Hamiltonian are fit in a scheme similar to that generating on-the-fly machine learning force field (MLFF) [30] with some modifications for effective Hamiltonian. The parameters are fitted during effective Hamiltonian MD simulations on relatively small cells, as described below.

(1) The energy, forces and stress tensor on the structure as well as their uncertainty are predicted by the effective Hamiltonian with the current parameters.

(2) The decision of FP calculation is made. If it is decided to be necessary to run FP calculation, go to step 3. Otherwise, go to step 5.

(3) The FP calculation is executed, and the results are stored into the train set.

(4) The parameters are fit using the updated train set.

(5) An MD step is executed to update the structure. If FP calculation is performed in this step, the forces and stress from the FP calculation is used. Otherwise, the forces and stress from the effective Hamiltonian are used.

The details of the effective Hamiltonian, the algorithms for fitting the parameters and predicting the uncertainty are explained below.

B. Effective Hamiltonian

The effective Hamiltonian of perovskites ABX₃ is developed based on the Taylor expansion of small distortions around the reference structure (typically ideal cubic perovskite structure). The degrees of freedom considered for the distortions are: (1) the local soft mode \mathbf{u}_i in each five-atom perovskite unit cell i , which is directly proportional to the local electric dipole in unit cell i [4]; (2) the pseudovector $\boldsymbol{\omega}_i$

centered at B site, characterizing the BX₆ octahedral tilting, also known as antiferrodistortive (AFD) distortions [7]; (3) the local variable \mathbf{v}_i characterizing the inhomogeneous strain around the unit cell i [4]; (4) the homogeneous strain tensor η_H [4]; and (5) the variable σ_i representing the atom occupation in unit cell i in complex perovskites [for example, in Pb(Sc, Ta)O₃ (PST) $\sigma_i = 1$ (respectively, 2) represents a Sc (respectively, Ta) atom occupying the B site in unit cell i] [6]. Note that the \mathbf{u}_i and \mathbf{v}_i vectors could be chosen to be centered at either A site or B site for different materials. In complex perovskites with multiple elements in B site [36], the potential energy of the effective Hamiltonian contains two main parts [6]

$$E_{\text{pot}} = E_{\text{ave}}(\{\mathbf{u}_i\}, \{\mathbf{v}_i\}, \{\boldsymbol{\omega}_i\}, \eta_H) + E_{\text{loc}}(\{\mathbf{u}_i\}, \{\mathbf{v}_i\}, \{\boldsymbol{\omega}_i\}, \{\sigma_i\}, \eta_H), \quad (1)$$

where the E_{ave} is the energy of the virtual A(B)X₃ system in which the different B -site atoms are averaged as virtual $\langle B \rangle$ atoms, and E_{loc} is the local perturbation to the virtual average system due to the distribution of the real B -site atoms. Note that different from previous works (see, e.g., Refs. [6, 7, 20, 37]) in which the virtual crystal approximation (VCA) [38] is imposed to represent the average A(B)X₃ system and compute the parameters in E_{ave} , here, the parameters of both the above terms are together fitted in the on-the-fly machine learning scheme, and VCA is not necessary in the computations.

The E_{ave} contains two main terms

$$E_{\text{ave}} = E_{\text{dip}}(\{\mathbf{u}_i\}, \{\mathbf{v}_i\}, \eta_H) + E_{\text{AFD}}(\{\mathbf{u}_i\}, \{\mathbf{v}_i\}, \{\boldsymbol{\omega}_i\}, \eta_H). \quad (2)$$

The E_{dip} is the energy of the local soft mode, strain and their couplings, which has the form [4]

$$E_{\text{dip}} = \sum_i [\kappa_2 u_i^2 + \alpha u_i^4 + \gamma(u_{ix}^2 u_{iy}^2 + u_{iy}^2 u_{iz}^2 + u_{iz}^2 u_{ix}^2)] + E_{\text{long}}(\{\mathbf{u}_i\}) + \frac{1}{2} \sum_{ij\alpha\beta} J_{ij\alpha\beta} u_{i\alpha} u_{j\beta} + \sum_{lm} N B_{lm} \eta_{H,l} \eta_{H,m} + E_{\text{elas},I}(\{\mathbf{v}_i\}) + \frac{1}{2} \sum_{i\alpha\beta} B_{i\alpha\beta} \eta_{i,l} u_{i\alpha} u_{i\beta}, \quad (3)$$

where α, β are Cartesian components along the x, y, z axes (which are chosen to be along the pseudocubic [100], [010] and [001] directions, respectively), $l, m = 1, 2, \dots, 6$ are Voigt notations [4]. The first term is the local mode self energy, where $u_i = |\mathbf{u}_i|$. The second term [4]

$$E_{\text{long}} = \frac{1}{2} \sum_{ij\alpha\beta} Q_{ij\alpha\beta} u_{i\alpha} u_{j\beta} \quad (4)$$

is the long range dipole-dipole interaction, in which the summations of both i and j run over all the unit cells in the supercell. The $Q_{ij\alpha\beta}$ is the dipole interaction matrix which is

obtained using Ewald summation [4, 39]. The third term is the short range interaction between neighbor local modes, in which the summation of i runs over all the unit cells and that of j runs only the neighbor unit cells around the cell i (up to the third nearest neighbor). The fourth term is the elastic energy of the homogeneous strain. The fifth term is the elastic energy of the inhomogeneous strain, which is given by [4]

$$E_{\text{elas},I} = \sum_i \left\{ \gamma_{11} [v_x(\mathbf{R}_i) - v_x(\mathbf{R}_i \pm \mathbf{x})]^2 + \gamma_{12} [v_x(\mathbf{R}_i) - v_x(\mathbf{R}_i \pm \mathbf{x})][v_y(\mathbf{R}_i) - v_y(\mathbf{R}_i \pm \mathbf{y})] + \gamma_{44} [v_x(\mathbf{R}_i) - v_x(\mathbf{R}_i \pm \mathbf{y}) + v_y(\mathbf{R}_i) - v_y(\mathbf{R}_i \pm \mathbf{x})]^2 + \text{cyclic permutations} \right\}, \quad (5)$$

where $\mathbf{x} = a_0 \hat{\mathbf{x}}, \mathbf{y} = a_0 \hat{\mathbf{y}}, \mathbf{z} = a_0 \hat{\mathbf{z}}$, and \pm indicates multiple terms to be summed. The parameters are defined as $\gamma_{11} = B_{11}^i/4, \gamma_{12} = B_{12}^i/8, \gamma_{44} = B_{44}^i/8$, where the superscript i denotes ‘‘inhomogeneous’’. Different from Ref. [4] where the B_{lm}^i parameters are simply equivalent to the B_{lm} parameters that related to the homogeneous strain, here they are fitted *independently*. Such fitting could be implemented conveniently benefited from the on-the-fly machine learning scheme employed here. Note that it is numerically found in our tests that the ‘‘elastic constants’’ corresponding to the inhomogeneous strain (B_{lm}^i parameters) could significantly differ from the B_{lm} parameters, and using the approximation in Ref. [4] exactly would lead to large errors on the B_{lm} parameters. The last term is the interaction between the soft mode and strain, in which the strain $\eta_{i,l} = \eta_{H,l} + \eta_{I,l}$ gathers both the homogeneous and inhomogeneous strains. The forms of $J_{ij\alpha\beta}, B_{lm}$ and $B_{l\alpha\beta}$ are greatly simplified due to the symmetry of the reference structure [4].

The E_{AFD} in Eq. (2) is the energy of AFD as well as the couplings with local soft mode and strain, which takes the form

$$E_{\text{AFD}} = \sum_i [\kappa_A \omega_i^2 + \alpha_A \omega_i^4 + \gamma_A (\omega_{ix}^2 \omega_{iy}^2 + \omega_{iy}^2 \omega_{iz}^2 + \omega_{iz}^2 \omega_{ix}^2)] + \frac{1}{2} \sum_{ij\alpha\beta} K_{ij\alpha\beta} \omega_{i\alpha} \omega_{j\beta} + \sum_{ij\alpha\beta\gamma\delta} K'_{ij\alpha\beta\gamma\delta} \omega_{i\alpha} \omega_{i\beta} \omega_{j\gamma} \omega_{j\delta} + \sum_{i\alpha} K'' \omega_{i\alpha}^3 (\omega_{i+\alpha,\alpha} + \omega_{i-\alpha,\alpha}) + \sum_{i\alpha\beta} C_{l\alpha\beta} \eta_{i,l} \omega_{i\alpha} \omega_{j\beta} + \sum_{ij\alpha\beta} D_{ij\alpha\beta} \omega_{i\alpha} \omega_{i\beta} u_{j\alpha} + \sum_{ij\alpha\beta\delta\gamma} E_{ij\alpha\beta\gamma\delta} \omega_{i\alpha} \omega_{i\beta} u_{j\gamma} u_{j\delta}, \quad (6)$$

where $\alpha, \beta, \gamma, \delta$ are Cartesian components along the x, y, z axes. The first term is the onsite contribution of AFD, where

$\omega_i = |\omega_i|$, which is proposed in Ref. [7]. The second term is the bilinear interaction between the AFD in site i and in the neighbor site j (up to the nearest neighbor), which is proposed in Ref. [7]. Note that the onsite and bilinear intersite parameters are not independent. The constraint $\kappa_A + 2k_1 = 0$ (using the notations of Ref. [40]) is imposed, as indicated by Ref. [41], which is also satisfied in previous works [40, 42] [43]. The third term is the biquadratic interaction between the AFD in site i and its nearest neighbor j . Such term is similar to the biquadratic term K' proposed in Ref. [44]. However, in this work, all the six different terms allowed by the symmetry (instead of only one isotropic term dependent on k_{21} in [44]) are considered. The fourth term is the anharmonic interaction between the AFD in nearest neighbor [45], where $\omega_{i+\alpha,\alpha}$ is the α component of the AFD mode at nearest neighbor site along the α Cartesian axis to the site i . The fifth term is the coupling between AFD and strain as proposed by Ref. [7]. The sixth and seventh terms are the trilinear and biquadratic coupling between AFD and local modes, which are proposed by Refs. [7] and [45], respectively. Note that the trilinear coupling (that dependent on the $D_{ij\alpha\beta}$ parameter) is only included if the local mode is centered at A site [45].

For the E_{loc} term in Eq. (1), the following form is used

$$E_{\text{loc}} = \sum_{ij} [Q_{ij}(\sigma_j) \mathbf{e}_{ji} \cdot \mathbf{u}_i + R_{ij}(\sigma_j) \mathbf{f}_{ji} \cdot \mathbf{v}_i] + \sum_i [\Delta \kappa_2(\sigma_i) u_i^2 + \Delta \alpha(\sigma_i) u_i^4 + \Delta \gamma(\sigma_i) (u_{ix}^2 u_{iy}^2 + u_{iy}^2 u_{iz}^2 + u_{iz}^2 u_{ix}^2)] + \sum_{i\alpha\beta} \Delta B_{l\alpha\beta}(\sigma_i) \eta_{i,l} u_{i\alpha} u_{j\beta} + \sum_{i\alpha\beta} \Delta C_{l\alpha\beta}(\sigma_i) \eta_{i,l} \omega_{i\alpha} \omega_{i\beta} + \sum_{ij\alpha\beta} \Delta D_{ij\alpha\beta}(\sigma_i) \omega_{i\alpha} \omega_{i\beta} u_{j\alpha} + \sum_{ij\alpha\beta\delta\gamma} \Delta E_{ij\alpha\beta\gamma\delta}(\sigma_i) \omega_{i\alpha} \omega_{i\beta} u_{j\gamma} u_{j\delta}, \quad (7)$$

where the summation of i runs over all the unit cells in the supercell, the summation j runs over the neighbor sites around i , \mathbf{e}_{ji} is the unit vector jointing the B site j and the center of local soft mode \mathbf{u}_i , and \mathbf{f}_{ji} is the unit vector jointing the B site j and the center of local variable \mathbf{v}_i . The first term characterizes the intersite interactions induced by distribution of B-site atoms, which is proposed by Ref. [6] and is associated with the ‘‘random electric field’’ and/or ‘‘random strain field’’ which is believed to have important effect in compounds with hetero valence B-site elements [16, 46]. The second term is the on-site contribution of alloying (using the terminology of Ref. [6]), as proposed by Refs. [6, 37]. The third and fourth term are the alloying effect on the coupling between strain and local soft mode and AFD, respectively. The fifth and sixth term are the alloying effect on the trilinear and biquadratic interaction between local soft mode and AFD, respectively. Among them, a similar form of the fifth term has been proposed in Ref. [47], while the other terms are proposed and

used for the first time in this work, to the best of our knowledge. Note that if the local mode \mathbf{u} is centered at A site, the $\Delta\kappa_2(\sigma_i)$, $\Delta\alpha(\sigma_i)$, $\Delta\gamma(\sigma_i)$, $\Delta B_{l\alpha\beta}(\sigma_i)$ parameters should be replaced by their average values over the 8 neighbor B sites. Note also that, for a specified materials, some of the above terms in Eqs.(6) and (7) may not be used since their effects are not important.

C. Mode and basis

Before describing the parametrization, let us further clarify the degrees of freedom (also called ‘‘modes’’) considered in the effective Hamiltonian, which is essential for bridging the effective Hamiltonian and the first-principles calculations. The mode is the local collective displacement of atoms in a specified pattern, which is also called lattice Wannier function (LWF) [4, 48]. In perovskites, the LWF basis of local dipole motion \mathbf{u} is chosen to be the local phonon mode having Γ_{15} symmetry centered on A or B site [19]. Typically, the LWF basis is determined from the eigenvector associated with the soft mode of the force constant or dynamic matrix of cubic perovskite, which takes the form $\boldsymbol{\xi} = (\xi_A, \xi_B, \xi_{X1}, \xi_{X2})$. For example, the displacement of local mode motion $u_{i\alpha}$ centered at B site consists of the displacement of center B atom by amounts of $u_i\xi_A$, the displacement of eight neighbor A atom by amounts of $u_i\xi_B$, and the displacement of the six neighbor X atom by amounts of $u_i\xi_{X1}$ or $u_i\xi_{X2}$, all along the α direction. The local motion \mathbf{v} is similar to \mathbf{u} but with the basis corresponding to the translation motion of all the atoms in the unit cell, i.e. with $\xi_A = \xi_B = \xi_{X1} = \xi_{X2}$.

The AFD mode $\boldsymbol{\omega}$ is kind of different from the \mathbf{u} and \mathbf{v} modes, since the neighbor BX_6 octahedra share the same X atom, and thus the $\boldsymbol{\omega}$ modes are not completely independent from each other. The actual movement of the X atom shared by the i and j sites associated with the AFD mode is given by

$$\Delta\mathbf{r}_X = \frac{a_0}{2}\hat{\mathbf{R}}_{ij} \times (\boldsymbol{\omega}_i - \boldsymbol{\omega}_j), \quad (8)$$

where $\hat{\mathbf{R}}_{ij}$ is the unit vector jointing the site i and site j . By the definition of Eq. (8), there are multiple (actually, infinite) different sets of $\{\boldsymbol{\omega}\}$ modes representing the same atomic structure (i.e. with the same set of atomic displacement) [41]. For example, it is clear that adding an arbitrary amount of $\boldsymbol{\omega}_0$ to all of the AFD modes does not change the displacement $\Delta\mathbf{r}_X$, since the displacement only depends on the *difference* between $\boldsymbol{\omega}_i$ and $\boldsymbol{\omega}_j$. To eliminate such arbitrariness, we typically impose the following extra restrictions on the AFD vectors and its cyclic permutations:

$$\forall x_0, \quad \sum_{i, n_x(i)=x_0} \omega_{i,x} = 0, \quad (9)$$

where i is the index of unit centered at $n_x(i)\hat{x}a_0 + n_y(i)\hat{y}a_0 + n_z(i)\hat{z}a_0$, where $\hat{x}, \hat{y}, \hat{z}$ are unit vectors along the x, y, z axes, and a_0 is the lattice constant of the five-atom perovskite unit cell. The summation runs over all the sites in the same layer marked with $n_x(i) = x_0$. Note that our definition of atomic

displacement [Eq. (8)] is identical to that in Ref. [41] [Eq. (1) there in], but our formalism is different from that of Ref. [41] by the extra restrictions [Eq. (9)].

It is clear from above that all of the \mathbf{u}, \mathbf{v} and $\boldsymbol{\omega}$ modes are linked *linearly* with atomic displacement about the reference structure. For a periodic supercell containing $N = L_x \times L_y \times L_z$ five-atom perovskite unit cells, the relation between the modes and atomic displacements could be written as

$$\mathbf{M}\mathbf{s} = \mathbf{x}, \quad (10)$$

where \mathbf{s} is a $9N$ column vector containing the modes $\mathbf{u}, \mathbf{v}, \boldsymbol{\omega}$ in each unit cell, \mathbf{x} is a $15N$ column vector containing the atomic displacement of each atom in the supercell, and \mathbf{M} is the matrix containing the information of LWF basis. The force acting on the *mode* could then be obtained from the chain rule

$$f_{s,i} = -\frac{\partial E_{\text{pot}}}{\partial s_i} = -\sum_j \frac{\partial E_{\text{pot}}}{\partial x_j} M_{ji}. \quad (11)$$

This equation can be written in matrix form as

$$\mathbf{f}_s = \mathbf{M}^T \mathbf{f}_x, \quad (12)$$

where \mathbf{f}_s and \mathbf{f}_x gather the forces acting on the modes and atoms, respectively.

Similar to the second-principle lattice dynamics formalism [49, 50], the actual atom coordinates in a supercell with homogeneous strain $\boldsymbol{\eta}_H$ and *atomic* displacement is defined as

$$\mathbf{r}_{lk} = (\mathbb{1} + \boldsymbol{\eta})(\mathbf{R}_l + \boldsymbol{\tau}_k) + \mathbf{x}_{lk}, \quad (13)$$

where $\mathbb{1}$ is the 3×3 identity matrix, $\boldsymbol{\eta}$ is the homogeneous strain (in 3×3 matrix format), \mathbf{R}_l is lattice vector corresponding to the unit cell l , $\boldsymbol{\tau}_k$ is the coordinate of atom inside the unit cell. Thus, the stress compatible with that calculated from FP should be obtained using the chain rule

$$\sigma_m = -\frac{\partial' E_{\text{pot}}}{\partial' \eta_m} = -\frac{\partial E_{\text{pot}}}{\partial \eta_m} - \sum_{lk\alpha} \frac{\partial E_{\text{pot}}}{\partial x_{lk\alpha}} \frac{\partial x_{lk\alpha}}{\partial \eta_m}, \quad (14)$$

as described in Appendix A of Ref. [50]. Practically in this work, such relation is used *inversely*. The stress $-\partial' E_{\text{pot}}/\partial' \eta_m$ obtained from the FP calculations are converted to $-\partial E_{\text{pot}}/\partial \eta_m$, compatible with the direct definition of the effective Hamiltonian.

D. Formalism of parametrization

In our parametrization approach, the parameters directly related to the long-range dipolar interaction E_{long} [Eq. (4)] [i.e. the lattice constant a_0 , the soft mode Born effective charge Z^* and optical dielectric constant ϵ_∞ (using the notations of Ref. [4])] are determined directly from the first principles calculations, while other parameters are determined through the on-the-fly machine learning process. It is clear from above that the effective Hamiltonian could be written in the following form

$$E_{\text{pot}} = E_{\text{long}} + \sum_{\lambda=1}^M w_\lambda t_\lambda(\{\mathbf{u}\}, \{\mathbf{v}\}, \{\boldsymbol{\omega}\}, \{\sigma\}, \boldsymbol{\eta}_H), \quad (15)$$

where E_{long} is fixed during the fitting process, M is the number of parameters to be fitted, w_λ is the parameter to be fitted (e.g., κ_2, α, γ mentioned above), and t_λ is the energy term dependent on the parameter w_λ , which is called symmetry-adapted term (SAT), using the terminology of Refs. [49, 50]. In other words, the energy apart from the long-range dipolar energy is *linearly* dependent on the *parameters*. Moreover, it is clear that the force (respectively, stress) have similar form to the energy, which is obtained by taking derivative over mode (respectively, strain) on E_{long} and t_λ . Such linearity is similar to the second-principle lattice dynamics [50] and MLFF with Gaussian approximation potential [51], allowing the application of similar regression algorithms. Here, we use the Bayesian linear regression algorithm similar to that previously applied in the context of MLFF [30], but with several modifications for the effective Hamiltonian context, as described below.

Given the linearity above, the energy, force and stress for each structure a calculated from the effective Hamiltonian could be written in the following matrix form

$$\mathbf{y}_a = \mathbf{y}_a^{\text{long}} + \phi_a \mathbf{w}, \quad (16)$$

where \mathbf{y}_a is a vector containing the energy per unit cell with respect to the reference structure [52], the forces acting on the modes and the stress tensor (in total $m_a = 1 + 9N + 6$ elements); $\mathbf{y}_a^{\text{long}}$ contains the energy per unit cell, forces and stress associated with the E_{long} term; \mathbf{w} is a vector consists of all the parameters $w_\lambda, \lambda = 1, \dots, M$; and ϕ_a is an $m_a \times M$ matrix. The first row in made up by the SAT t_λ . The next $9N$ rows are made up by the negative derivatives of SAT over modes in each unit cell $-\partial t_\lambda / \partial s_{i\alpha}$ where s is u, v or ω , i is the unit cell index and α is the Cartesian axis. And the last 6 rows consists of the negative derivatives of SAT over homogeneous strain components $-\partial' t_\lambda / \partial' \eta_{H,l}$, where the prime indicates the chain rule in Eq. (14) should be used. Since the parameters depended by the E_{long} term are determined before the fitting process, the $\mathbf{y}_a^{\text{long}}$ is known for each given structure indexed a . Thus, the above equation could be rewritten as

$$\tilde{\mathbf{y}}_a \equiv \mathbf{y}_a - \mathbf{y}_a^{\text{long}} = \phi_a \mathbf{w}. \quad (17)$$

In the parametrization process, a set of structures are selected as the training set, and the structures are indexed by $a = 1, \dots, N_T$. First-principles calculations are performed on these structures to get the energy per unit cell, forces acting on the atoms, and stress tensor. The forces acting on the modes are then obtained by applying Eq. (12). The $\tilde{\mathbf{y}}_a$ vector of all the structures in the training set then constitute the vector \mathbf{Y} containing $\sum_a m_a$ elements. On the other hand, the ϕ_a matrices of the structures in the training set constitute the Φ matrix. In this form, the parametrization problem is to adjust \mathbf{w} to fit $\Phi \mathbf{w}$ against \mathbf{Y} . To balance the energy, force and stress values with different dimensions properly, they are typically divided by their standard deviation in the training set to get dimensionless values. Furthermore, an optional weight could be assigned to each of the types to adjust the preference between different fitting targets. Practically, this is achieved by left multiplying a diagonal matrix \mathbf{H} made up by h_i / σ_i to

Φ and \mathbf{Y}

$$\Phi \rightarrow \mathbf{H}\Phi, \quad \mathbf{Y} \rightarrow \mathbf{H}\mathbf{Y}, \quad (18)$$

where h_i and σ_i are the weight and standard deviation of the specified type of values (energy, force of different modes and stress), respectively.

Given two necessary assumptions satisfied (see Appendix B of Ref. [30]), the posterior distribution of the parameter is a multidimensional Gaussian distribution

$$p(\mathbf{w}|\mathbf{Y}) = \mathcal{N}(\bar{\mathbf{w}}, \Sigma), \quad (19)$$

where the center of the distribution

$$\bar{\mathbf{w}} = \frac{1}{\sigma_v^2} \Sigma \Phi^T \mathbf{Y} \quad (20)$$

is the desired optimal parameters, and the variance

$$\Sigma = \left[\frac{1}{\sigma_w^2} \mathbf{I} + \frac{1}{\sigma_v^2} \Phi^T \Phi \right]^{-1} \quad (21)$$

is a measure of the uncertainty of the parameters. Here, \mathbf{I} is the identity matrix, σ_v is a hyperparameter describing the deviation of FP data from the model prediction $\phi_a \mathbf{w}$, and σ_w is a hyperparameter describing the covariance of the prior distribution of parameter vector \mathbf{w} (see Appendix B of Ref. [30] for more details).

Given the observation of the training set, the posterior distribution of the energy, forces and stress of a new structure is also shown to be a Gaussian distribution [30]

$$p(\tilde{\mathbf{y}}|\mathbf{Y}) = \mathcal{N}(\phi \bar{\mathbf{w}}, \sigma), \quad (22)$$

where the covariance matrix

$$\sigma = \sigma_v^2 \mathbf{I} + \phi \Sigma \phi^T \quad (23)$$

measures the uncertainty of the prediction on the new structure. Following Ref.[30], the diagonal elements of the second term is used as the Bayesian error. If the Bayesian error is large, the prediction on the energy, forces and stress by current effective Hamiltonian model is considered unreliable, then new FP calculation is required to fit the parameters.

The hyperparameters σ_v and σ_w are determined by evidence approximation [30, 53], in which the marginal likelihood function corresponding to the probability of observing the FP data \mathbf{Y} with σ_v and σ_w is maximized [see Eq. (31) and Appendix C in Ref. [30]]. Practically, the hyperparameters σ_v and σ_w are calculated along with Σ and $\bar{\mathbf{w}}$ by executing self-consistent iterations at each time when FP data for a new structure is collected.

The Bayesian linear regression described above is equivalent to the ridge regression [34, 54] in which the target function

$$\mathcal{O} = \|\Phi \mathbf{w} - \mathbf{Y}\|^2 + \lambda \|\mathbf{w}\|^2 \quad (24)$$

is minimized, where λ is the Tikhonov parameter which is equivalent to σ_v^2 / σ_w^2 here [34, 54]. The main purpose of imposing the Tikhonov parameter is to prevent overfitting [54].

However, in the context of effective Hamiltonian parametrization, there are only a small amount of parameters to be determined (typically several tens), while the number of values collected from FP calculations are typically much larger, which means the linear equations $\Phi \mathbf{w} = \mathbf{Y}$ is greatly overdetermined. In such case, the regularization is usually not necessary. If the regularization term $\lambda \|\mathbf{w}\|$ in Eq. (24) is removed, the problem becomes a simple linear least square fitting, and the parameter could be simply solved by

$$\mathbf{w} = \Phi^+ \mathbf{Y}, \quad (25)$$

where Φ^+ is the Moore-Penrose pseudoinverse of the matrix Φ , which could be computed by performing the singular-value decomposition of Φ [55]. Indeed, our numerical tests show that the resulting parameter from such fitting without regularization is pretty close to that obtained by Bayesian linear regression. Similar observation is also reported in the context of MLFF with Gaussian approximation potential model (or its analogs) [55, 56]. On the other hand, in effective Hamiltonian, unlike Gaussian approximation potential, the parameters in \mathbf{w} have different dimensions, and it is hard to balance the *values* between different parameters, indicating the regularization may be not suitable for effective Hamiltonian. Based on the two reasons above, in our fitting scheme, it is typically assumed that $\sigma_w \rightarrow \infty$, and thus the equivalent Tikhonov regularization parameter λ approaches zero, and the fitting scheme is equivalent to the linear least square fitting.

E. Decision to perform FP calculation

In each effective Hamiltonian MD step in the fitting process, the Bayesian error of the energy, forces and stress predicted by the effective Hamiltonian is calculated by Eq. (23) and compared to the threshold to determine whether FP calculation is necessary. The threshold is updated dynamically during the fitting process. The flow for updating the threshold and determining whether FP calculation will be performed is similar to that in Ref. [30], with the exception that the spilling factor is not used in this work.

Another difference between the scheme employed here and that proposed in Ref. [30] is that, the parameters are typically fitted *immediately* as soon as when new FP calculation is performed, instead of fitted after several FP results are obtained. This difference stems from the observation that the parameter fitting for the effective Hamiltonian is typically very fast compared to the FP calculations. Such immediate fitting is helpful for reducing the number of FP calculations required and improve the fitting efficiency.

Note that we have also tried another strategy for weighting different values and making the decision of FP calculation, which is similar to that used in the FLARE package [33, 57]. In this strategy similar to FLARE, the covariance of the deviation between FP data and model prediction σ_v [see Eq. (B1) in Ref. [30]] is allowed to take different values for energy, forces acting on the \mathbf{u} , \mathbf{v} and $\boldsymbol{\omega}$ modes, and diagonal and off-diagonal elements of the stress tensor (in total 6 different values). Thus, the \mathbf{I}/σ_v matrix is replaced by a diagonal matrix

Λ comprised by the 6 different values at proper places, and Eq. (20) becomes

$$\bar{\mathbf{w}} = \Sigma \Phi^T \Lambda^T \Lambda \mathbf{Y}. \quad (26)$$

Comparing Eqs. (26) and (18), it is clear that the matrix Λ takes the place of \mathbf{H} . In other words, the Λ matrix serves as the weight of different type of values (energy, force or stress) and makes the \mathbf{Y} vector dimensionless at the same time. Under this assumption, the equation for calculating σ_v [Eq. (C2) in Ref. [30]] is not valid anymore [53], and the 6 different σ_v values are obtained by numerically minimizing the marginal likelihood function [33, 53]. It seems to be a good idea to get the weight automatically in this strategy. However, the tests show that the resulting parameters are usually less accurate (i.e. shows relative larger deviation between the energy calculated from FP calculations and that predicted by the final parameter after fitting), and it is harder to find the correct ground state structure during the MD runs in the fitting process. The possible reason is the hyperparameter σ_v for different values can *change greatly* during the on-the-fly machine learning process, especially when the number of structures in the training set is relatively small, leading to possibly inappropriate weighting between different values. If the σ_v for energy is estimated to a large value, the weight of energy is small, and the resulting parameter is inaccurate.

F. Multi B-site element perovskites

In our on-the-fly machine learning scheme, the parametrization of perovskites with more than one elements in B site is basically the same as that of single component ones. However, there are still some issues that may deserve special discussions. All of the parameters appearing in E_{loc} [Eq. (7)] are component-dependent, which may take different values for different components. For example, $Q(\sigma = 1)$ is typically not equal to $Q(\sigma = 2)$.

The component-dependent parameters could be divided into two types. The first type is the so-called ‘‘spring’’ parameter (using the terminology of Ref. [58]), containing the Q and R parameters in the first term of Eq. (7). The SATs dependent on such terms has no similar term in the E_{ave} . In most of previous practices (see, e.g. [21, 59, 60]) and from the original definition [61], the following summation rule is satisfied

$$\sum_{c=1}^{n_c} x(\sigma_c) Q_{ij}(\sigma_c) = 0, \quad (27)$$

where $c = 1, \dots, n_c$ is the component index, $x(\sigma_c)$ is the concentration ratio of the component c . Note that the Q parameters is assumed to be isotropic and only dependent on component σ and the distance between i, j . Thus, the above equation is applicable separately for the first, second and third nearest neighbors. Similar equations are valid for the R parameters. Thus, for a system with n_c different components in B site, there are $n_c - 1$ independent Q parameters for each

of considered neighbor pairs. These $n_c - 1$ independent parameters are treated *separately* as the w_λ parameters in Eq. (15). Another type, to be called modification parameters in this article, contains the rest of parameters in E_{loc} [Eq. (7)]. The terms dependent on such parameters have similar terms in E_{ave} . For example, the $\Delta\kappa_2(\sigma_i)u_i^2$ term in Eq. (7) has the same form as the $\kappa_2u_i^2$ term in Eq. (3). The $\Delta\kappa_2(\sigma_i)$ parameter serves as “modification” of the real atom occupation on the “original” $\Delta\kappa_2$ parameter. Practically, in the on-the-fly fitting process, these modification terms are merged with the “original” terms as $\kappa_2(\sigma_i) = \kappa_2 + \Delta\kappa_2(\sigma_i)$, the n_c independent parameters of the latter one are treated separately as the w_λ parameters in Eq. (15).

As mentioned above, the Z^* , ϵ_∞ and a_0 parameters are determined directly from first-principles calculations before the on-the-fly machine learning process. Such calculations rely on the selection of reference structure (which serves as the center of Taylor expansion in the effective Hamiltonian, as described in Sec. II B) and the determination of LWF basis. For simple perovskites with only one element in A and B sites, such work is straightforward. The reference structure is usually the five-atom cubic perovskite with optimized lattice constant, which has $Pm\bar{3}m$ symmetry. The calculations could be simply completed by following the process introduced in Ref. [19]. In some previous works for multi A - or B -site element perovskites [6, 7, 20, 37], this is achieved by applying virtual crystal approximation (VCA) [38], in which different atoms in one site are treated as an average virtual atom, and the $Pm\bar{3}m$ symmetry of the cubic perovskite structure is reserved and the other processes are performed as in Ref. [19]. However, as already addressed by previous works [38, 62, 63] and our tests, the applicability and accuracy of VCA are limited, especially for hetero valence elements. Regarding this, VCA is not used in this work [64]. In such case, the selection of reference structure, determination of LWF basis are not trivial tasks as they seem to be, due to the symmetry broken caused by the atom occupation. One can understand this by noting that the standard cubic cell may *not* be an energy local minimum for some atomic distributions (especially those with low symmetry). Moreover, as the degrees of freedom in a single five-atom unit cell is reduced from 15 (3 for each atom) to 9 (the three three-dimensional mode vectors \mathbf{u} , \mathbf{v} and $\boldsymbol{\omega}$) in the effective Hamiltonian, there are infinity number of different atomic structures with all zero modes, which are all possible candidates for the reference structure. It is suggested [65] that fitting effective Hamiltonian with all “secondary distortions” (i.e. the 6 degrees of freedom not considered in the effective Hamiltonian) that *minimizing* the energy may be better than that with all secondary distortions are *frozen at zero*. Considering this, the standard cubic perovskite structure may not be the best choice for the reference structure.

To determine the reference structure and LWF basis of a multi B -site element system, a relatively small supercell (typically $2 \times 2 \times 2$ supercell with 40 atoms) with a specified atomic distribution is selected. Usually atomic distribution with relatively high symmetry (for example, rocksalt-ordered distribution for two-component system with 1:1 concentration) or low energy (as predicted by charge model [66], nearest neighbor

model [67] or direct FP calculations) is preferred. The LWF basis of soft mode is determined from the eigenvector of the “approximate” cubic force constant matrix (in which the forces acting on the atoms sitting at the same sublattice are averaged), or from the direct fitting against atom displacement of a low energy structure (as obtained by performing direct first-principles structural relaxation calculations).

Once the LWF basis is determined, the reference structure is obtained by performing first-principles *constrained* structural relaxation, in which all the considered modes in the effective Hamiltonian (\mathbf{u} , \mathbf{v} and $\boldsymbol{\omega}$) are kept zero. Such constraint is applied by projecting the forces acting on the atoms to the space spanned by the secondary distortions in each ionic step during the structural relaxation. In other words, the forces in the space spanned by the \mathbf{u} , \mathbf{v} and $\boldsymbol{\omega}$ modes are removed to keep such modes zero in the resulting relaxed structure. Practically, the atom force in the space spanned by the considered modes is [see also Eq. (12)]

$$\mathbf{f}_x' = (\mathbf{M}^T)^+ \mathbf{f}_s = (\mathbf{M}^T)^+ \mathbf{M}^T \mathbf{f}_x. \quad (28)$$

Removing such part from the total force \mathbf{f}_x yields

$$\mathbf{f}_x'' = \mathbf{f}_x - \mathbf{f}_x' = (\mathbf{I} - (\mathbf{M}^T)^+ \mathbf{M}^T) \mathbf{f}_x. \quad (29)$$

The constrained relaxation is then practically realized by replacing \mathbf{f}_x with \mathbf{f}_x'' in each ionic step during the structural relaxation.

The ordering of cation is shown to play an important role in some multi B -site component complex perovskites, such as $\text{PbSc}_{0.5}\text{Ta}_{0.5}\text{O}_3$ (PST) and $\text{PbSc}_{0.5}\text{Nb}_{0.5}\text{O}_3$ [68]. In such case, different cation ordering should be considered in the parametrization of effective Hamiltonian. To do this, supercells with several different distribution of atoms should be employed in the fitting process. For each cation distribution, the constrained cell relaxation should be performed to get the reference structure. On-the-fly machine learning is *sequentially* employed on these structures to fit the parameters.

III. COMPUTATIONAL DETAILS

On-the-fly machine learning for parametrization of effective Hamiltonian is performed on $2 \times 2 \times 2$, $2 \times 2 \times 4$ or $2 \times 4 \times 4$ supercells (corresponding to 40, 80 or 160 atoms). The MD simulations are performed with isothermal-isobaric (NPT) ensemble using Evans-Hoover thermostat [69, 70], with integration step of 1 fs. Typically, each MD simulation on a given structure is executed for 20 ps. For each MD step the FP calculation is required by the on-the-fly machine learning process, first-principles self-consistent calculation within density functional theory (DFT) is performed. All the FP calculations are performed using the VASP package [71, 72] with projector augmented wave (PAW) method [73]. The local density approximation (LDA) in the parametrization of Ceperly and Alder [74] or solid-revised Perdew-Burke-Ernzerhof (PBEsol) [75] functional is used. The $3 \times 3 \times 3$, $3 \times 3 \times 2$ and $3 \times 2 \times 2$ k-point meshes are used for the supercells with 40, 80 and 160 atoms, respectively, and the plane wave

cutoff of 550 eV is employed. The optical dielectric constant is computed using the density functional perturbation theory (DFPT) [76]. The Born effective charge of the local mode is obtained by fitting the polarization against the local mode amplitude, where the polarization is computed using the Berry phase method [77].

Typically, the following steps are employed to fit the parameters for a specified material with multi B -site elements.

(1) On-the-fly fitting is first employed on a $2 \times 2 \times 2$ supercell (40 atoms) with ordered B -site atoms. The MD simulation starts from the reference structure. A set of parameters is obtained along with the MD trajectory.

(2) (Optional) Continue the fitting with $2 \times 2 \times 2$ supercell to improve the accuracy of the parameters. This process may be repeated with different temperatures or starting structures. The FP results collected in previous fitting process are read and used for fitting the parameters along with the newly collected ones.

(3) On-the-fly fitting is employed on a $2 \times 4 \times 4$ supercell (160 atoms) with ordered B -site atoms. The MD simulation starts from the reference structure. All the previously collected FP results are used. Note that this fitting on the relatively large cell is necessary for the j_5 and j_7 parameters in the short-range interaction between the second and third nearest neighbor soft mode vectors. These parameters are always zero if 40-atom cells are used. [78].

(4) On-the-fly fitting is employed on a $2 \times 2 \times 2$ or $2 \times 2 \times 4$ supercells (40 or 80 atoms) with *disordered* B -site atoms. All the previously collected FP results are used. This step is necessary for fitting the intersite interaction parameters that dependent on the component, especially for the spring parameters Q and R [see the first term of Eq. (7)]. Note that such terms have no effect in the two-component system with perfectly ordered B -site atoms.

IV. EXAMPLE OF APPLICATION

This on-the-fly learning scheme described above is applied to several perovskites, including simple perovskite BaTiO_3 with only one element in A and B sites, and double perovskite $\text{Pb}(\text{Sc}, \text{Ta})\text{O}_3$ (PST) with two elements in the B site, and the obtained parameters correctly reproduce the phase transition sequence previously reported in experiments or calculations [10, 79, 80]. Here, we show the PST example with more details.

The lead scandium tantalate $\text{PbSc}_{0.5}\text{Ta}_{0.5}\text{O}_3$ (PST) is a relaxor oxide of considerable importance due to its broad dielectric response, large pyroelectric and electrocaloric effect [81–83]. Previous works shows that the phase transition behavior of PST is affected by the ordering degree of Sc^{3+} and Ta^{5+} cations. PST with highly ordered B -site cations exhibits a sharp first order phase transition from high temperature cubic paraelectric phase to low temperature rhombohedral ferroelectric phase near room temperature. With the decreasing of ordering degree, the transition temperature decreases and the phase transition becomes diffuse [68, 79]. In our previous work [80], the effective Hamiltonian is developed for PST, in

which the parameters are computed directly from the FP calculations using conventional methods with the help of VCA. Such effective Hamiltonian have successfully reproduced the phase transition and electrocaloric effect of PST, as well as their evolution with the change of B -site ordering degree.

Here, the local mode $\{\mathbf{u}\}$ is chosen to be centered at A site, and the $\{\mathbf{v}\}$ mode is centered at B site. The energy, stress, and forces acting on different modes are weighted equally. The LDA functional is used in the FP calculations. During the MD simulations, the following quantities are calculated. (i) The supercell averaged local mode $\mathbf{u} = \frac{1}{N} \sum_i \mathbf{u}_i$, which is directly proposed to the polarization. (ii) The AFD vector at R point $\boldsymbol{\omega}_R = \frac{1}{N} \sum_i \omega_i (-1)^{n_x(i)+n_y(i)+n_z(i)}$, characterizing the anti-phase octahedra tilting.

After the determination of LWF basis, reference structure, and parameters directly related to the dipolar interactions from direct FP calculations, on-the-fly machine learning is first performed on rocksalt-ordered PST. The $2 \times 2 \times 2$ and $2 \times 4 \times 4$ supercells (corresponding to 40 and 160 atoms, respectively) are used in turn. After that, the $2 \times 2 \times 4$ supercell (80 atoms) with disordered B -site atoms is used.

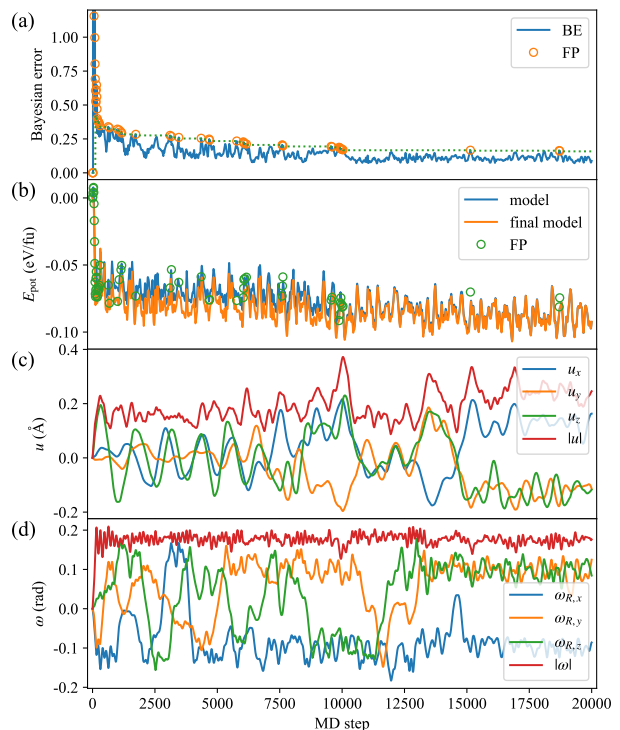


FIG. 1. Properties extracted from the learning process of rocksalt-ordered PST (first round) as functions of MD step. (a) Bayesian error (solid line). Circles denote the steps at which the FP calculations are performed. Dash line denote the threshold to perform FP calculations. (b) Potential energy per formula unit (fu) predicted during the learning process (blue line), calculated by the final parameter after the fitting (orange line) and that from the FP calculations (circles). (c) Local soft mode \mathbf{u} in the fitting process. (d) AFD mode $\boldsymbol{\omega}$ in the fitting process.

An example of the typical evolution during on-the-fly ma-

chine learning run is depicted in Fig. 1. Figure 1(a) shows the Bayesian error during the fitting process. At the beginning (about 300 steps), the Bayesian error is quite large, and FP calculations are called frequently. As the fitting progresses, more FP data are collected and the parameters are updated, leading to the rapid decline of Bayesian error. The threshold is also adjusted dynamically in this process. After about 1000 MD steps, the threshold is nearly unchanged and the FP calculations are only rarely required. Figure 1(b) shows the potential energy predicted by the effective Hamiltonian and that computed from FP calculations in the simulation, showing they are close to each other at each step. Figures 1(c) and (d) show the mode evolution during the simulation. In the first several thousand steps, the soft mode \mathbf{u} vibrates around the zero, while the AFD at R point ω_R typically have finite values but change over time. After about 15000 steps, both \mathbf{u} and ω_R enter a relatively stable status, both show approximately equal finite values along the x, y, z axes, indicating the spontaneous polarization along the pseudocubic [111] direction and octahedra tilting pattern $a^-a^-a^-$ (in Glazer's notation [84]). Such rhombohedral ferroelectric phase is consistent with the ground state observed in the experiments [79].

To check the validity of the parameters, Monte Carlo (MC) simulations are performed using the effective Hamiltonian parameters calculated from direct FP calculations (as used in Ref. [80]) and that obtained from on-the-fly fitting in present work. The MC simulations are performed on $12 \times 12 \times 12$ supercell (corresponding to 8640 atoms) with rocksalt-ordered Sc and Ta atoms using Metropolis algorithm [85]. The simulations start from relatively high temperature and cool down with small temperature steps. Typically, 100 000 Monte Carlo sweeps are executed for each temperature, where the last 50 000 sweeps are used for collecting the statistical average values. For the temperatures near the phase transition point, more Monte Carlo sweeps (up to 400 000) are employed. Figure 2(a) shows the soft mode \mathbf{u} and AFD at R point ω_R as functions of temperature, computed using the parameters fitted from direct FP calculations. At high temperature, the average values of both \mathbf{u} and ω_R vanishes, indicating the average cubic paraelectric phase. As the temperature down to 280 K, both \mathbf{u} and ω_R show equal finite values along x, y, z axes, suggesting a rhombohedral ferroelectric phase with octahedra tilting pattern $a^-a^-a^-$ and spontaneous polarization along the pseudocubic [111] direction. As shown in Fig. 2(b), the phase transition predicted by the parameters fitted from the on-the-fly machine learning is rather similar to that predicted from the parameters from direct FP calculations, with

slightly lower phase transition temperature of 245 K. Such predicted phase transitions are in reasonably consistent with experiments [81], confirming the validity of the parametrization scheme.

Note that as in the previous work [80], the negative pressure -6.5 GPa is applied for the effective Hamiltonian model directly calculated from the FP calculations. Similarly, negative pressure of -3 GPa is applied for that fitted from the present on-the-fly machine learning process. Such negative pressures are applied to correct the underestimating of lattice constant by the LDA functional [4].

V. SUMMARY

In summary, on-the-fly machine learning scheme is developed to obtain the parameters of the effective Hamiltonian. The parameters are computed during MD simulations. The energy, forces and stress as well as their Bayesian errors are predicted at each MD step based on the effective Hamiltonian and FP data collected before, and FP calculations are called to fit the parameter when the Bayesian errors are large. The fitting procedure based on Bayesian linear regression provides not only the values of the parameters, but also their uncertainties. For complex perovskites with multi element in A or B site, the component-dependent parameters are fitted in simultaneously with other parameters, without the need of using VCA. Such learning scheme offers a new alternative to parametrize the effective Hamiltonian in a universal and highly automatic process, and is especially suitable for the systems that have complex interaction terms and/or complex components. This parametrization scheme is applied to PST. The parameters fitted for PST correctly reproduces its phase transition, which demonstrates the validity of this on-the-fly machine learning scheme.

ACKNOWLEDGMENTS

X.M., Y.Y. and D.W. thank the National Key R&D Programs of China (grant NOs. 2020YFA0711504, 2022YFB3807601), the National Natural Science Foundation of China (grant NOs. 12274201, 51725203, 51721001, 52003117 and U1932115) and the Natural Science Foundation of Jiangsu Province (grant NO. BK20200262). We are grateful to the HPCC resources of Nanjing University for the calculations.

[1] P. Hohenberg and W. Kohn, *Phys. Rev.* **136**, B864 (1964).
 [2] W. Kohn and L. J. Sham, *Phys. Rev.* **140**, A1133 (1965).
 [3] R. M. Martin, *Electronic Structure: Basic Theory and Practical Methods* (Cambridge University Press, 2004).
 [4] W. Zhong, D. Vanderbilt, and K. M. Rabe, *Phys. Rev. B* **52**, 6301 (1995).
 [5] P. Ghosez and J. Junquera, *Annu. Rev. Condens. Ma. P.* **13**, 325 (2022).

[6] L. Bellaïche, A. García, and D. Vanderbilt, *Phys. Rev. Lett.* **84**, 5427 (2000).
 [7] I. A. Kornev, L. Bellaïche, P.-E. Janolin, B. Dkhil, and E. Suard, *Phys. Rev. Lett.* **97**, 157601 (2006).
 [8] P. Chen, C. Paillard, H. J. Zhao, J. Íñiguez, and L. Bellaïche, *Nat. Commun.* **13**, 2566 (2022).
 [9] L. Chen, B. Xu, Y. Yang, and L. Bellaïche, *Adv. Funct. Mater.* **30**, 1909496 (2020).

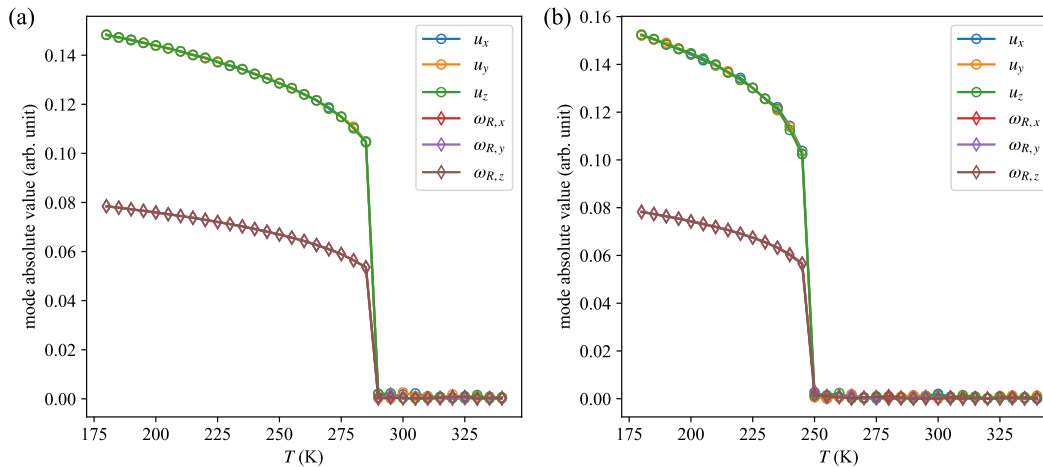


FIG. 2. Phase transition of rocksalt-ordered PST computed from the effective Hamiltonian (a) using the parameters from direct FP calculations; (b) using the parameters from on-the-fly fitting.

- [10] W. Zhong, D. Vanderbilt, and K. M. Rabe, *Phys. Rev. Lett.* **73**, 1861 (1994).
- [11] Y. Nahas, S. Prokhorenko, J. Fischer, B. Xu, C. Carrétéro, S. Prosandeev, M. Bibes, S. Fusil, B. Dkhil, V. Garcia, and L. Bellaiche, *Nature* **577**, 47 (2020).
- [12] Y. Nahas, S. Prokhorenko, L. Louis, Z. Gui, I. Kornev, and L. Bellaiche, *Nat. Commun.* **6**, 8542 (2015).
- [13] D. Wang, A. A. Bokov, Z.-G. Ye, J. Hlinka, and L. Bellaiche, *Nat. Commun.* **7**, 11014 (2016).
- [14] Y. Nahas, A. Akbarzadeh, S. Prokhorenko, S. Prosandeev, R. Walter, I. Kornev, J. Íñiguez, and L. Bellaiche, *Nat. Commun.* **8**, 15944 (2017).
- [15] I. Ponomareva and S. Lisenkov, *Phys. Rev. Lett.* **108**, 167604 (2012).
- [16] Z. Jiang, Y. Nahas, S. Prokhorenko, S. Prosandeev, D. Wang, J. Íñiguez, and L. Bellaiche, *Phys. Rev. B* **97**, 104110 (2018).
- [17] N. Choudhury, L. Walizer, S. Lisenkov, and L. Bellaiche, *Nature* **470**, 513 (2011).
- [18] A. M. George, J. Íñiguez, and L. Bellaiche, *Nature* **413**, 54 (2001).
- [19] R. D. King-Smith and D. Vanderbilt, *Phys. Rev. B* **49**, 5828 (1994).
- [20] A. Al-Barakaty, S. Prosandeev, D. Wang, B. Dkhil, and L. Bellaiche, *Phys. Rev. B* **91**, 214117 (2015).
- [21] L. Bellaiche, A. García, and D. Vanderbilt, *Ferroelectrics* **266**, 41 (2002).
- [22] L. Walizer, S. Lisenkov, and L. Bellaiche, *Phys. Rev. B* **73**, 144105 (2006).
- [23] M. R. Chellali, A. Sarkar, S. H. Nandam, S. S. Bhattacharya, B. Breitung, H. Hahn, and L. Velasco, *Scr. Mater.* **166**, 58 (2019).
- [24] D. Miracle and O. Senkov, *Acta Mater.* **122**, 448 (2017).
- [25] G. Tallarita, R. Licheri, S. Garroni, R. Orrù, and G. Cao, *Scr. Mater.* **158**, 100 (2019).
- [26] Y. Zhang, T. T. Zuo, Z. Tang, M. C. Gao, K. A. Dahmen, P. K. Liaw, and Z. P. Lu, *Prog. Mater. Sci.* **61**, 1 (2014).
- [27] H. Pan, F. Li, Y. Liu, Q. Zhang, M. Wang, S. Lan, Y. Zheng, J. Ma, L. Gu, Y. Shen, P. Yu, S. Zhang, L.-Q. Chen, Y.-H. Lin, and C.-W. Nan, *Science* **365**, 578 (2019).
- [28] H. Pan, S. Lan, S. Xu, Q. Zhang, H. Yao, Y. Liu, F. Meng, E.-J. Guo, L. Gu, D. Yi, X. R. Wang, H. Huang, J. L. MacManus-Driscoll, L.-Q. Chen, K.-J. Jin, C.-W. Nan, and Y.-H. Lin, *Science* **374**, 100 (2021).
- [29] Y. Pu, Q. Zhang, R. Li, M. Chen, X. Du, and S. Zhou, *Appl. Phys. Lett.* **115**, 223901 (2019).
- [30] R. Jinnouchi, F. Karsai, and G. Kresse, *Phys. Rev. B* **100**, 014105 (2019).
- [31] R. Jinnouchi, J. Lahnsteiner, F. Karsai, G. Kresse, and M. Bokdam, *Phys. Rev. Lett.* **122**, 225701 (2019).
- [32] E. V. Podryabinkin and A. V. Shapeev, *Comput. Mater. Sci.* **140**, 171 (2017).
- [33] J. Vandermause, S. B. Torrisi, S. Batzner, Y. Xie, L. Sun, A. M. Kolpak, and B. Kozinsky, *npj Comput. Mater.* **6**, 20 (2020).
- [34] R. Jinnouchi, K. Miwa, F. Karsai, G. Kresse, and R. Asahi, *J. Phys. Chem. Lett.* **11**, 6946 (2020).
- [35] P. Friederich, F. Häse, J. Proppe, and A. Aspuru-Guzik, *Nat. Mater.* **20**, 750 (2021).
- [36] In this work, we focus on the cases where the B site may contain multi elements while the A site contains only one element. For the cases where A site contains multiple elements, the effective Hamiltonian may need to be modified, while the following on-the-fly fitting scheme is still valid.
- [37] A. R. Akbarzadeh, S. Prosandeev, E. J. Walter, A. Al-Barakaty, and L. Bellaiche, *Phys. Rev. Lett.* **108**, 257601 (2012).
- [38] L. Bellaiche and D. Vanderbilt, *Phys. Rev. B* **61**, 7877 (2000).
- [39] D. Wang, J. Liu, J. Zhang, S. Raza, X. Chen, and C.-L. Jia, *Comput. Mater. Sci.* **162**, 314 (2019).
- [40] Y. Yang, B. Xu, C. Xu, W. Ren, and L. Bellaiche, *Phys. Rev. B* **97**, 174106 (2018).
- [41] D. Vanderbilt and W. Zhong, *Ferroelectrics* **206**, 181 (1998).
- [42] Y. Yang, H. Xiang, and L. Bellaiche, *Phys. Rev. B* **104**, 174102 (2021).
- [43] Note that in Refs. [40, 42], such constraint appeared to be $\kappa_A + 4k_1 = 0$. Such difference stems from the $1/2$ factor in Eq. (6) in this study.
- [44] J. Zhang, Y. Zhang, T. Xu, and J. Wang, *Phys. Rev. B* **103**, 014113 (2021).
- [45] S. Prosandeev, D. Wang, W. Ren, J. Íñiguez, and L. Bellaiche, *Adv. Funct. Mater.* **23**, 234 (2013).

- [46] J. Íñiguez and L. Bellaiche, *Phys. Rev. B* **73**, 144109 (2006).
- [47] B. Xu, D. Wang, J. Íñiguez, and L. Bellaiche, *Adv. Funct. Mater.* **25**, 552 (2015), <https://onlinelibrary.wiley.com/doi/pdf/10.1002/adfm.201403811>.
- [48] K. M. Rabe and U. V. Waghmare, *Phys. Rev. B* **52**, 13236 (1995).
- [49] J. C. Wojdeł, P. Hermet, M. P. Ljungberg, P. Ghosez, and J. Íñiguez, *J. Phys.: Condens. Matter* **25**, 305401 (2013).
- [50] C. Escorihuela-Sayalero, J. C. Wojdeł, and J. Íñiguez, *Phys. Rev. B* **95**, 094115 (2017).
- [51] A. P. Bartók, M. C. Payne, R. Kondor, and G. Csányi, *Phys. Rev. Lett.* **104**, 136403 (2010).
- [52] Note that in the effective Hamiltonian formalism, the potential energy of the reference structure is zero by definition (see Sec. II B). Thus, the energy obtained from the FP calculations should be subtracted by the energy of the reference structure to be consistent with the effective Hamiltonian.
- [53] C. M. Bishop, *Pattern Recognition and Machine Learning*, soft-cover reprint of the original 1st edition 2006 (corrected at 8th printing 2009) ed., Information Science and Statistics (Springer New York, 2016).
- [54] Z.-H. Zhou, *Machine learning* (Springer, 2021).
- [55] C. Verdi, F. Karsai, P. Liu, R. Jinnouchi, and G. Kresse, *npj Comput. Mater.* **7**, 156 (2021).
- [56] P. Liu, C. Verdi, F. Karsai, and G. Kresse, *Phys. Rev. Mater.* **5**, 053804 (2021).
- [57] J. Vandermause, Y. Xie, J. S. Lim, C. J. Owen, and B. Kozinsky, *Nat. Commun.* **13**, 5183 (2022).
- [58] F. Mayer, M. N. Popov, P. Ondrejko, J. Hlinka, J. Spitaler, and M. Deluca, *Phys. Rev. B* **106**, 224109 (2022).
- [59] S. Prosandeev, S. Prokhorenko, Y. Nahas, A. Al-Barakaty, L. Bellaiche, P. Gemeiner, D. Wang, A. A. Bokov, Z.-G. Ye, and B. Dkhil, *Phys. Rev. B* **102**, 104110 (2020).
- [60] S. Prosandeev, D. Wang, A. R. Akbarzadeh, and L. Bellaiche, *J. Phys.: Condens. Matter* **27**, 223202 (2015).
- [61] S. de Gironcoli, P. Giannozzi, and S. Baroni, *Phys. Rev. Lett.* **66**, 2116 (1991).
- [62] J. S. Baker and D. R. Bowler, *Phys. Rev. B* **100**, 224305 (2019).
- [63] C. Eckhardt, K. Hummer, and G. Kresse, *Phys. Rev. B* **89**, 165201 (2014).
- [64] Note that, in principle, it is still possible to use VCA within our on-the-fly machine learning framework.
- [65] O. Diéguez, O. E. González-Vázquez, J. C. Wojdeł, and J. Íñiguez, *Phys. Rev. B* **83**, 094105 (2011).
- [66] L. Bellaiche and D. Vanderbilt, *Phys. Rev. Lett.* **81**, 1318 (1998).
- [67] J. Zhang, L. Liu, A. A. Bokov, N. Zhang, D. Wang, Z.-G. Ye, and C.-L. Jia, *Phys. Rev. B* **103**, 054201 (2021).
- [68] C. G. F. Stenger and A. J. Burggraaf, *Phys. Status Solidi A* **61**, 653 (1980).
- [69] I. Ponomareva, L. Bellaiche, T. Ostapchuk, J. Hlinka, and J. Petzelt, *Phys. Rev. B* **77**, 012102 (2008).
- [70] W. G. Hoover, A. J. C. Ladd, and B. Moran, *Phys. Rev. Lett.* **48**, 1818 (1982).
- [71] G. Kresse and J. Furthmüller, *Comput. Mater. Sci.* **6**, 15 (1996).
- [72] P. E. Blöchl, *Phys. Rev. B* **50**, 17953 (1994).
- [73] G. Kresse and D. Joubert, *Phys. Rev. B* **59**, 1758 (1999).
- [74] D. M. Ceperley and B. J. Alder, *Phys. Rev. Lett.* **45**, 566 (1980).
- [75] J. P. Perdew, A. Ruzsinszky, G. I. Csonka, O. A. Vydrov, G. E. Scuseria, L. A. Constantin, X. Zhou, and K. Burke, *Phys. Rev. Lett.* **100**, 136406 (2008).
- [76] X. Gonze and C. Lee, *Phys. Rev. B* **55**, 10355 (1997).
- [77] R. D. King-Smith and D. Vanderbilt, *Phys. Rev. B* **47**, 1651 (1993).
- [78] Note that, the cell of $2 \times 3 \times 3$ (90 atoms) is enough for producing non-zero j_5 and j_7 parameters. However, to be coherent with the AFD distortions, here $2 \times 4 \times 4$ cells are used.
- [79] N. Setter and L. E. Cross, *J. Appl. Phys.* **51**, 4356 (1980).
- [80] X. Ma, Y. Yang, L. Bellaiche, and D. Wu, *Phys. Rev. B* **105**, 054104 (2022).
- [81] B. Nair, T. Usui, S. Crossley, S. Kurdi, G. G. Guzmán-Verri, X. Moya, S. Hirose, and N. D. Mathur, *Nature* **575**, 468 (2019).
- [82] P. Lheritier, A. Torelló, T. Usui, Y. Nouchokgwe, A. Aravindhhan, J. Li, U. Prah, V. Kovacova, O. Bouton, S. Hirose, and E. Defay, *Nature* **609**, 718 (2022).
- [83] F. Chu, N. Setter, and A. K. Tagantsev, *J. Appl. Phys.* **74**, 5129 (1993).
- [84] A. M. Glazer, *Acta Crystallogr. Sect. B* **28**, 3384 (1972).
- [85] N. Metropolis, A. W. Rosenbluth, M. N. Rosenbluth, A. H. Teller, and E. Teller, *J. Chem. Phys.* **21**, 1087 (1953).